Bacterial predator–prey dynamics in microscale patchy landscapes

Hol, Felix J H; Rotem, Or; Jurkevitch, Edouard; Dekker, Cees; Koster, Daniel A.

DOI
10.1098/rspb.2015.2154

Publication date
2016

Document Version
Accepted author manuscript

Published in
Royal Society of London. Proceedings B. Biological Sciences

Title: Bacterial predator-prey dynamics in micro-scale patchy landscapes

Authors and affiliations:

Felix J.H. Hol[†], Or Rotem[‡], Edouard Jurkevitch[‡], Cees Dekker[†], Daniel A Koster[§,*]

† Department of Bionanoscience, Kavli Institute of Nanoscience, Delft University of Technology, Lorentzweg 1, 2628 CJ Delft, The Netherlands.

‡ Department of Agroecology and Plant Health, The Robert H. Smith Faculty of Agriculture, Food and Environment, The Hebrew University of Jerusalem, Jerusalem, Israel.

§ Department of Ecology, Evolution and Behavior, The Alexander Silberman Institute of Life Sciences, Edmond J. Safra campus, The Hebrew University of Jerusalem, 91904 Jerusalem, Israel.

* **Corresponding author**: Daniel A Koster: danikoster@gmail.com.

Abstract

Soil is a microenvironment with a fragmented (patchy) spatial structure in which many bacterial species interact. Here we explore the interaction between the predatory bacterium *Bdellovibrio bacteriovorus* and its prey *Escherichia coli* in microfabricated landscapes. We ask how fragmentation influences the prey dynamics at the microscale, and compare two landscape geometries: a patchy landscape and a continuous landscape. By following the dynamics of prey populations with high spatial and temporal resolution for many generations, we find that the variation in predation rates is twice as large in the patchy landscape and the dynamics is correlated over shorter length scales. We also find that while the prey population in the continuous landscape is almost entirely driven to extinction, a significant part of the prey population in the fragmented landscape persists over time. We observe significant surface-associated growth, especially in the fragmented landscape and we surmise that this sub-population is more resistant to predation. Our results thus show that microscale fragmentation can significantly influence bacterial interactions.

Keywords: bdellovibrio bacteriovorus/metapopulation/nanofabricated landscapes/predator-prey

Introduction

Bacterial habitats, such as soil, our gastrointestinal tract, and even the ocean are spatially structured at the micro-scale [1,2]. Soil typically contains particles with sizes that vary between 2 μm or less for clay and 1 mm for sand [3,4] (Fig 1a). It is within the confines of the interconnected cavities in between soil particles that microorganisms, such as bacteria, interact. Most of our knowledge of population dynamics in such highly structured landscapes comes from a large body of theoretical [5–7] and experimental studies [8–11] concerning macroscopic organisms in macroscopic landscapes. Due to technical challenges, however, experimental study and even a clear theoretical framework of the population dynamics of microorganisms in spatially structured microhabitats such as soil is lacking, especially for interacting bacterial populations such as predator-prey communities.

One may hypothesize that for bacteria, a landscape with constrictions with a size of only a few microns can be considered fragmented. This hypothesis predicts that the population dynamics differ significantly between individual patches and that the dynamics of interacting bacteria at the local (patch) level become decorrelated quickly with increasing distance [12]. Habitat fragmentation may also influence the lifetime of the population as a whole [5,8,12,13]. However, bacteria differ in important ways from "large" animals: bacteria grow to higher densities, possibly reducing stochastic fluctuations that may lead to local extinction. Bacteria are also highly mobile, in terms of their swimming speed [14] as well as in terms of their ability to pass through small constrictions [15]. Furthermore, while diffusion of signaling molecules, food, and waste is very efficient at microscopic scales, diffusion at larger scales is negligible. Finally, bacteria can adopt very different lifestyles, living clustered together in biofilms with greatly reduced mobility, or as motile planktonic individuals [16]. For these reasons, it is unclear whether bacterial habitats that are spatially structured at the micro-scale can be considered "fragmented" or not. Because macroscopic fragmentation has been shown to affect key parameters such as the global lifetime of a population [8–11] we believe there is reason to assume that microscopic fragmentation could be of importance for understanding bacterial life in natural structured habitats such as soil. However, the question of how fragmentation affects predator-prey dynamics at the micro-scale has remained unanswered.

Over the past few years, microfabrication techniques have allowed for the creation of micro-scale synthetic ecosystems that are structured at the spatial scales relevant to bacterial populations [17–21]. It thus has become technically feasible to quantify bacterial predator-prey interactions in each of the individual micron-scale patches of a landscape under controlled conditions over many generations. Taking advantage of these recent advances, we fabricated a micro-scale fragmented habitat and a non-fragmented habitat, and contrasted bacterial predator-prey dynamics in these two habitat types. We studied the bacterial predator

Bdellovibrio bacteriovorus preying upon *Escherichia coli*. *B. bacteriovorus* is a small (0.4x1μm) and highly motile (it can swim over 160 μm/s, or 160 body lengths per second [22]) predator of Gram-negative bacteria, that occurs *e.g.* in soil, in the human gut, and in water [23]. To complete its life cycle, *B. bacteriovorus* inserts itself into the periplasmic space of its prey, and converts it into a round-shaped "bdelloplast" [24]. *B. bacteriovorus* subsequently extracts and ingests solutes from its prey and increases in length, after which it divides and 4-6 progeny are produced per *E. coli* prey. Approximately 3-4 hours after invasion, *B. bacteriovorus* lyses its host and swims away to hunt for the next prey [23]. While *B. bacteriovorus* are ferocious predators, a small fraction of prey may survive predation due to plastic phenotypic resistance, preventing the total eradication of the prey population [25].

Studying the *B. bacteriovorus – E. coli* interaction in both fragmented and continuous landscapes allows us to test the hypothesis that a bacterial habitat featuring micro-scale constrictions is fragmented and as such influences the predator-prey interaction. Specifically, we address the question to what extent a spatially structured microhabitat gives rise to variations in predation rates, and at what scale predator-prey dynamics are spatially correlated in a micro-structured landscape such as soil. Can *B. bacteriovorus* predate effectively in spatially structured landscapes? Does fragmentation increase the persistence of the prey population? Furthermore, given that *B. bacteriovorus* has shown potential to protect crops, reduce biofouling, and to serve as a "living antibiotic" [26–29], it would be useful to know how its effectiveness in structured habitats, such as human tissue, relates to its effectiveness as measured in well-mixed (unstructured) culture flasks [30–32]. In this regard, *B. bacteriovorus* has also attracted significant interest because of its potential to eradicate bacterial biofilms which are spatially structured at the micro-scale [33,34].

Materials and methods

Strains and growth conditions

Growth of E. coli

We used strain JEK 1036 previously described in [18], which is wild-type *E. coli* W3110 labeled with a green fluorescent protein (lacZY::GFPmut2). JEK 1036 was grown O/N from glycerol in LB broth at 30° C shaken at 200 rpm, diluted 1000-fold the next morning in Diluted Nutrient Broth (DNB, 0.8 g/L NB, 2mM $CaCl_2 \cdot 2H_2O$, 3mM $MgCl_6 \cdot 2H_2O$, pH 7.6) and grown to OD_{600} ~1. Fluorescence expression was induced by adding 100 μM of Isopropyl β-D-1-thiogalactopyranoside (IPTG, Promega) to the medium.

Growth of Bdellovibrio bacteriovorus and microhabitat inoculation

E. coli JEK 1036 [18] was cultivated to maximum turbidity (OD_{600}~4) in LB broth, then concentrated to OD_{600}=10 by centrifugation and subsequently resuspended in HEPES buffer (25 mM HEPES, 2 mM $CaCl_2 \cdot 2H_2O$, 3 mM $MgCl_6 \cdot 2H_2O$, pH 7.8). *B. bacteriovorus* HD100, with a chromosomal fusion of the HuaA histone like protein gene [24] to monomeric Teal protein (mTeal), was added to this medium from glycerol stock, and was incubated O/N in a volume of 2 ml while shaking at 280 rpm at 28° C, until a transparent liquid was obtained. The culture's transparency indicates that all *E. coli*, except for a minute fraction that is phenotypically resistant, have been lysed. The culture was then spun down at 3000 rpm for 10 min and resuspended in 2 ml fresh DNB, at 28°C. The microhabitat was simultaneously inoculated with approximately 3 μl of resuspended *B. bacteriovorus* culture and approximately 3 μl of pure *E. coli* culture in DNB medium in a 1:1 ratio (measured by optical density) from opposite sides.

Experimental set-up

Microfabrication of microhabitats

To emulate the patchy geometry of natural bacterial habitats with relevant spatial dimensions (Fig. 1a), and to allow for the quantitative study of predator-prey interactions as a function of space and time, we created a well-defined linear array of habitat patches on a silicon chip, that are connected to each other by narrow corridors (Fig. 1b and d, top) [18,35]. As a control for the patchiness of the patchy geometry, we also designed a continuous landscape of identical volume that consists of one large habitat without internal constrictions (Fig. 1e). Microhabitats were fabricated in silicon using a two-step procedure of photolithography and reactive ion etching following a previously published protocol [18,35]. The patchy microhabitats consist of 85 patches (each 100 μm in length, 100 μm in width and 15 μm in depth) connected by corridors (50x5x15 μm), the continuous microhabitats consist of a single patch (8500x100x15 μm) with a total volume identical to the volume of the patchy habitat. The 180 nm deep slits are too shallow for the passage of bacteria and thus preclude them from leaving the microhabitats and entering the reservoirs. On the other hand, the slits do allow for the diffusion of *e.g.* nutrients and waste [18,35]. At the start of an experiment the reservoirs (having a volume ~15 times the habitat) are filled with fresh DNB medium (supplemented with 100 μM IPTG) to ensure that plenty of nutrients are available to the *E. coli* for the entire duration of the experiment. Two ports to inoculate bacteria were drilled through the silicon, one at each end of the habitat, furthermore, ports were drilled to allow for the filling of the reservoirs. After short exposure to O_2-plasma to facilitate proper bonding, a silicon microhabitat was bonded to a polydimethylsiloxane (PDMS) coated cover slip. The

microhabitats and reservoirs were then filled with fresh DNB medium (supplemented with 100 μM IPTG). Subsequently, cultures of *B. bacteriovorus* and *E. coli* were inoculated from opposite ends as described above. Medium in the device was not replenished during the experiment. After the habitat and reservoirs had been filled and the habitat had been inoculated with bacteria, the inlet holes were sealed with quick drying PDMS. Data was acquired for periods up to 3 days, the exact duration of each experiment is shown on the time axis of the relevant figures. All experiments were performed in triplicate.

Microhabitat imaging

To capture the dynamics of the prey population in the presence (and absence) of the predator, microhabitats were imaged every 20 minutes using an Olympus IX81 inverted microscope controlled with MicroManager 1.4.14 software [36], equipped with a 20x 0.75NA objective, an Andor Neo sCMOS camera, and a motorized stage (Marzhauser). The sample was illuminated using an X-cite 120 Q (Lumen dynamics) light source. We use the total fluorescence intensity in the GFP channel as a proxy for prey density which was previously shown to be a valid approach [35,37]. Due to the limited brightness of *B. bacteriovorus*, predator cells were not continuously monitored. The fluorescent mTeal fusion, however, allowed us to periodically verify the presence of *B. bacteriovorus* using a 100x objective. The set-up was enclosed in an incubator set to 28°C.

Image processing and data analysis

Images were processed in Matlab using a custom script. Briefly, each patch was subdivided in 98x98 regions (we left out a margin from the edges of the patches to remain unbiased by the limited precision of the microscope stage movement) from which fluorescence time traces were obtained by binning into bins of 3x3 pixels. By dividing the patches into subregions, we are able to quantify variation of predation rates *within* individual patches (see Results and below), while the binning reduces noise in the fluorescence signal. To render the analysis of the continuous landscape as comparable as possible to the patchy landscape, artificial "virtual patches" of identical size and inter-patch spacing were computationally generated in the continuous landscape during analysis (Fig 1b). In designing the habitat geometries, we chose to keep the total habitat volume of the patchy and continuous landscapes identical, and therefore, given the different geometries of the two landscapes, the continuous landscape consists of 55 "virtual patches" *vs.* 85 patches for the patchy landscape. Next, we performed a background correction for each time trace and smoothed time traces using a 5-point window. Subsequently, the maximal predation rates were calculated for each time trace by calculating the maximal negative slope (maximal predation rate) beyond the maximum value of a time trace (Figure 2a and Figure 3a). Using this algorithm, each of the patches yields 10^4 values for

the maximal predation rates. We exclude time traces originating from empty regions within the patch (typically a few percent of the traces, defined by a maximum that is 10% or less than the most frequent maximal value of all time traces in the patch). The values for the maximal predation rates were then plotted in histograms such as the blue histograms in Figure 2b and 3b. To usefully compare the variance of this distribution between patches, also in cases where the mean values differ, we divide the maximal predation rate by its mean. We thus describe the variation as the coefficient of variation (CV), defined as the standard deviation of the distribution divided by the mean of the distribution. The within-patch CV thus obtained for each patch was averaged over all patches yielding two values: one for all of the patches in the patchy geometry ($CV_{l,p}$), and one for all of the "virtual patches" in the continuous geometry ($CV_{l,c}$). To compare the local CV of the patches with the CV of the landscape as a whole, we generate two more numbers: one that describes the global CV for the entire landscape for a patchy geometry ($CV_{g,p}$) and one that describes the global CV of the entire landscape for the continuous geometry ($CV_{g,c}$). The degree to which the global CV for the entire landscape and that of the individual patches (local CV) differ is expressed in terms of their ratio R according to R= Global CV/Local CV for each repeat experiment where a ratio equal to one means that the variation at the local scale is equal to the variation at the global scale. This analysis yields 6 ratios: three repeat measurements for the patchy landscape R_p and three repeat measurements for the continuous landscape R_c. To test whether R_p and R_c differ significantly, we use a Wilcoxon rank-sum test.

Spatial Correlation

To calculate the spatial correlation between patches, time traces were used as shown in Figure 1, where a single fluorescence time trace represents the dynamics in a single patch. Spatial correlations were calculated as a function of increasing inter-patch distance using the corrcoef function in Matlab.

Survival Analysis

For the survival analysis, we used the fluorescence signal originating from all 98x98 subregions in the patches. As is described in the "Results" section, the typical fluorescence signal rises first (due to bacterial growth) and subsequently reaches a maximum, after which it declines (due to predation). First, the time-point associated with the maximum value in the fluorescence is determined. Second, the time-point at which the fluorescence crosses the cutoff fluorescence value associated with a region that does not contain any bacteria is determined. This time-point is recorded and designated as the "time-of-death" for that particular region in space. This procedure is repeated for all time traces, and Kaplan-Meier survival curves are generated using the log-rank function of Matlab. As the patchy- and

continuous-habitat experiments were performed in triplicate, we obtain three sets of survival curves (supplementary figure), each quantifying the surviving population fractions in the patchy and continuous landscapes over time. The log-rank algorithm determines this fraction, as well as whether the two survival curves for the patchy and continuous landscapes are statistically different, including the associated *p*-value. Additionally, the algorithm determines the residual values, i.e. the population fraction that persists.

The survival analysis as described above was also performed separately for the periphery (the outer rim of the habitat patch, measuring 15 μm or less to the closest sidewall) and center (the remaining 70x70x10 μm^3 central volume element) of habitat patches. The center of the habitat patches has a low surface to volume ratio (0.20 μm^{-1}) as only a top and bottom surface are present, whereas the periphery is enclosed by the sidewalls increasing the surface to volume ratio (0.28 μm^{-1} and 0.27 μm^{-1} for the patchy and continuous habitats respectively).

Real-time movies

Real-time and time-lapse movies provide additional insights beyond those extracted from total fluorescence intensity time traces. For example, movies help to identify different modes of prey growth such as surface-associated growth, which manifests itself as an increase in fluorescence at the edges of an observed microcolony in combination with limited (or even the absence of) motility. Furthermore, the process and timing of predation can be followed. While we are unable to observe the exact time of entry of the predator, we do clearly observe the formation of bdelloplasts when rod-shaped prey is converted into round-shaped bdelloplasts, followed by their sudden disappearance due to lysis (Movies S1, S4 and S5).

Results

Prior to studying the dynamics between predator and prey, we perform a control experiment in which the landscape is only inoculated with prey (Fig. 1b and c). This experiment shows that *E. coli* quickly populates the entire landscape, though some spatial variation is present (Figure 1b). The mean fluorescence intensity of all patches over time (Figure 1c) shows that the prey initially grows exponentially, until it reaches stationary phase ~10 h after inoculation. In the following 30 hours the population does not collapse, as evidenced by an approximately constant mean fluorescent intensity. We conclude that in the absence of predator, and in good agreement with previous studies of *E. coli* in microfabricated landscapes [18,38], the bacterial prey population inoculated in the microfabricated landscape exhibits all familiar phases of growth and does not show population collapse even after two days.

A different picture emerges when predator and prey are both inoculated from opposite sides. Figure 1 shows prey dynamics as a function of space and time in the presence of the predator, for the patchy landscape (Fig. 1d) and for the continuous landscape (Fig. 1e). An experiment is typically characterized by four phases in the predator-prey dynamics (labeled (*i*) through (*iv*) in Fig. 1d). Initially, (phase (*i*)), growth of the prey population is dominant over predation and consequently the population density increases. During phase (*i*), the majority of *E. coli* bacteria are planktonic, motile, and migrate between patches rapidly, whereas in phase (*ii*), the majority of *E. coli* become sessile and show an increase in surface associated growth [16]. Without predator (Figure 1b and c), one observes phases (*i*) and (*ii*) only (see [38] for a detailed analysis of the colonization process). When prey and predator are both (simultaneously) inoculated, predation starts to dominate in phases (*ii*) and (*iii*) and the population density of *E. coli* starts to decline approximately 10-20 hours after inoculation. In the final phase (*iv*), the prey density reaches a steady-state, where most of the prey population is eradicated, except for a small number of prey that is presumably characterized by plastic phenotypic resistance to predation [25]. We note that while the specific spatial pattern, *e.g.* the presence of two separated predation foci in the patchy landscape in Fig. 1d, varies from experiment to experiment (see Supplemental Figure), all six independent experiments showed the four phases described above. Supplemental Movie S1 shows the predation process in more detail, including the formation of round bdelloplasts and their sudden disappearance as they get lysed by *B. bacteriovorus*. We conclude that *B. bacteriovorus* do indeed predate *E. coli* populations in the structured landscapes and that the prey population is driven towards extinction.

We then ask how habitat topology influences the variation of prey dynamics at local *vs.* global spatial scales. To address this, we first quantify how much the maximal predation rate of the prey population varies *within* patches in the patchy landscape (local scale), where the conditions are presumably uniform, and compare this quantity to the spread of the maximal decay rate *across* patches (global scale). To compare spreads with slightly different means, we use the coefficient of variation (CV) as a measure of the spread (see the "Image processing and data analysis" section of the Materials and Methods for details). We calculate four values of the CV: 1) $CV_{l,p}$ (local, patchy; variation within patches in the patchy landscape), 2) $CV_{g,p}$ (global, patchy; variation in the entire patchy landscape), 3) $CV_{l,c}$ (local, continuous; variation within the virtual "patches" in the continuous landscape) and 4) $CV_{g,c}$ (global, continuous; variation in the entire continuous landscape). The values obtained, as well as a schematic representation of the regions for which the CVs are calculated, are summarized in Table 1.

	Mean±SEM	Scale	Graphical representation
$\mathbf{CV_{l,p}}$	0.51±0.06	local	 <CV> of all patches in patchy landscape
$\mathbf{CV_{g,p}}$	1.53 ±0.66	global	 CV of entire patchy landscape
$\mathbf{CV_{l,c}}$	0.55±0.06	local	 <CV> of all "patches" in continuous landscape
$\mathbf{CV_{g,c}}$	0.74±0.08	global	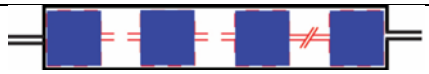 CV of entire continuous landscape

Table 1. Local and global coefficients of variation in the patchy and continuous landscape. Values are the mean ± the standard error of the mean (SEM) of three independent experiments.

First, we observe that in the patchy landscape the variation within a patch (local scale) is smaller than the variation between patches ($CV_{l,p} < CV_{g,p}$). A statistical comparison of $CV_{l,p}$ and $CV_{g,p}$ is provided below. This observation is consistent with the notion that conditions that affect predator-prey dynamics, *e.g.* fluctuations in predator and prey densities, vary across patches in a patchy landscape. The source of the increased variation across the landscape is not obvious as both the limited migration due to the patchiness of the landscape and the increasing physical distance between ever more distant regions could contribute to this result. To uncouple the influences of the patchy structure and physical distance, we compare the patchy landscape to the continuous landscape that does not contain structural patchiness. We find that the local CV of the decay rates within the "virtual patches" in the continuous landscape, $CV_{l,c}$, is 0.55 ± 0.06, very similar to the local CV in the patchy landscape ($CV_{l,p} \approx CV_{l,c}$). This similarity is expected since both distributions represent local dynamics within an identical area (and volume) in the landscapes. The maximal decay rates of all time traces across the entire continuous landscape (red traces in Fig. 3c), have a relatively narrow distribution (Figure 3d) and has a global $CV_{g,c}$ of 0.74±0.08. This number is larger than the average local $CV_{l,c}$ of the "virtual patches" in the continuous landscape, indicating that conditions in the entire continuous landscape are somewhat more diverse than in a small fraction of the entire landscape. However, it is important to note that the global $CV_{g,c}$ of the

continuous landscape is considerably smaller than the global $CV_{g,p}$ of the patchy landscape ($CV_{g,p}$ = 1.53 $\pm$0.66).

To properly address the question whether the patchiness of the patchy landscape increases variation, we calculate the ratios $R_p = CV_{g,p}/CV_{l,p}$ for the patchy landscape and $R_c = CV_{g,c}/CV_{l,c}$ for the continuous landscape. This assessment shows that R_p is indeed larger than R_c (R_p=2.8$\pm$0.9, R_c=1.3$\pm$0.02 mean $\pm$ SEM of n = 3 experiments, $R_p > R_c$ p = 0.05, using a single-sided Wilcoxon rank-sum test). We may thus conclude that our findings support the hypothesis that patchiness increases the variation in population decay rates of the prey by approximately a factor of two.

While the measurements described above show that patchiness influences the predator-prey interaction at the global level, these measurements do not provide insight into the extent to which the prey dynamics is correlated in space. Spatial correlation gives insights into the connectivity between patches and the ease at which bacteria can move between patches. To quantify this we analyze the correlation between the time-traces of patches as a function of patch distance. Figure 4a shows the dependence on distance of the Pearson's correlation coefficient, for the patchy (red) and continuous (black) landscapes (see the 'Spatial Correlation' section of the Materials and Methods). As expected, both landscapes show a decrease in correlation with increasing distance. However, while the two landscapes lose correlation similarly for distances up to approximately 15 patches, this analysis also shows that the patchy landscape loses correlation faster than the continuous landscape beyond 15 patches. Spatial dynamics in the patchy landscape thus extend beyond a single patch, yet are correlated over shorter distances than in the continuous landscape, a high migration rate of bacteria between adjacent patches in the initial phases of the experiment may explain correlations beyond the patch size. A high migration rate between patches would be expected to contribute to a high coupling between patches and synchronization in the dynamics between patches. Indeed, real-time movies of the initial phases of the experiment (Movie S2 and S3) show that up to hundreds of bacteria can migrate between patches per minute, depending on bacterial density. This finding suggests that the migration rate in the patchy landscape is apparently sufficiently high to generate correlation in the dynamics between a few adjacent patches, but over long (>15 patches) distances, the effects of the patchy landscape on the dynamics become apparent. As such, the present spatial configuration represents an unexplored intermediate regime between a coherent well-mixed state and an entirely fragmented state [12].

Given our finding that patchiness affects variation and spatial correlation of the prey dynamics, we now ask what the ramifications of these findings are for the survival of prey. Does patchiness, like in various macroscopic systems [5,8,12,13] give rise to an increased persistence of the prey population, or do specific bacterial properties (such as high mobility,

high density, and surface growth) render the analogy to macroscopic organisms invalid? To answer this question, we perform a survival analysis for prey in both the patchy and continuous landscapes. Using fluorescence as a proxy for prey persistence we generated survival curves representing the spatial fraction of the prey population that survives (see Fig. 4b and the 'Survival Analysis' section of the Materials and Methods for details). After the onset of predation (in this experiment app. after 10 h), survival curves in both the patchy and continuous landscape start to decline. Interestingly, the survival functions of the patchy and continuous populations are not equal, (p<0.00001 using a log-rank test). Survival curves for all the experiments are displayed in the Supplementary Figure g-i. These results show that while almost the entire population dies in the continuous landscape (residual value=0.04$\pm$0.04, n=3), a significant fraction of the population in the patchy landscape survives (0.36$\pm$0.10, n=3) demonstrating that prey survival in the patchy landscape is increased compared to the continuous landscape (p=0.05, using a single-sided Wilcoxon rank-sum test). The increased survival in the patchy landscape is not caused by a lower per capita predation rate as the absolute values for the per capita predation rates are 0.06$\pm$0.01 and 0.05$\pm$0.01 per hour for the patchy geometry and continuous landscapes respectively, in good agreement with previously measured batch values [30–32]. This control shows that a) the geometry of the landscape does not influence the kinetics of the predator-prey interaction and that b) the rates measured in the microchip are comparable to those previously measured.

Discussion

This work was inspired by studies macro-scale patchy landscapes showing that patchiness can greatly impact the spatiotemporal dynamics of predator-prey systems, such as an extended lifetime of a macroscopic population (Holyoak and Lawler, 1996; Dey and Joshi, 2006; Sutcliffe *et al.*, 1997; Ellner *et al.*, 2001)). We investigated to what extent bacterial predator-prey systems in micro-fragmented landscapes exhibit similar behaviors. The present patchy landscape can be considered "mildly" fragmented as on the one hand fragmentation increases the variation in predation rates, but on the other hand spatial correlations extend over multiple patches. The presence of this intermediate regime should perhaps be considered in the context of the fundamental differences between macroscopic animals inhabiting macroscopic landscapes and microscopic organisms inhabiting microscopic landscapes. First, compared to macroscopic animals, bacteria (and especially *B. bacteriovorus*) move through space fast and grow to high densities. If one were to simply scale up the microfragmented landscape and its microbial inhabitants to macroscopic proportions, one would obtain the following (rather absurd) large-scale animal equivalent: hundreds of cheetahs racing at approximately 500 km/h in random directions while hunting on a few hundred antelopes that run around at 100 km/h in a square field of only 100m x 100m. Such exceedingly high density

and mobility would likely give rise to relatively homogeneous spatial dynamics within the field and result in spatial correlations that extend beyond it. Moreover, bacteria can adopt distinct lifestyles, existing as individual planktonic cells that swim freely, or growing as multi-cellular surface-associated colonies. Bacteria exhibiting one of these two lifestyles differ in myriad ways including cellular mobility, capacity to forage, resistance to environmental insults, and physiology. By impacting core processes like colonization, survival, and extinction; lifestyles switching plays a central role in bacterial ecology. Another distinction between the microscopic and macroscopic worlds is that signaling molecules, nutrients, and waste diffuse across space highly efficiently. For example, a small molecule such as glucose traverses the length of a patch (100 μm) in approximately 10 s and a distance of 15 patches in approximately an hour (which is on the order of one bacterial division time). Such environmental homogenization may be less apparent for macroscopic animals. A future theory of microbial ecology that draws from macroscopic theory would have to take into account these fundamental differences.

Perhaps the most salient effect described in this manuscript is the observation that a significant fraction of prey in the fragmented landscape persists, in contrast to the prey population in the continuous landscape that is nearly eradicated. As this effect cannot be attributed to a difference in predation rates (the maximal predation rates in the two landscapes are equal), the increased persistence may be attributed to the geometry of the patchy landscape. Classical metapopulation dynamics, in which a given patch becomes extinct after which it is "rescued" by migration of prey from an adjacent patch, could be responsible for the increased survival in the patchy landscape. However, while this scenario cannot be ruled out completely, the limited extend to which lateral movement (migration) is visible in the kymographs leads us to favor a different explanation.

Previous work has shown that while *B. bacteriovorus* can predate an *E. coli* biofilm a significant fraction of the biofilm often remains [39], in contrast to predation on planktonic *E. coli* cultures where only a minute fraction of the population survives due to phenotypic resistance. In the microhabitats under investigation here, part of the prey population grows as a surface-associated biofilm (see Movies S1, S4 and S5). Surface-associated growth concentrates in the periphery of habitat patches where, due to the presence of sidewalls, the surface to volume ratio is higher when compared to the center of habitat patches. An increase in the population fraction adopting a surface-associated lifestyle may render it more resistant to predation and could result in an increased survival in the periphery of patches. To test this hypothesis, we performed a survival analysis for the periphery and center of habitat patches separately. This analysis revealed that prey persistence in the patchy habitat is indeed significantly higher in the periphery compared to the center of patches (peripheral residual fraction of 0.49 ± 0.14, versus 0.30 ± 0.10, $p<0.02$ using a one-tailed paired t-test). In contrast,

we did not observe a significant difference when comparing survival in the periphery and center of (virtual) patches in the continuous habitat (0.05 ± 0.05 and 0.04 ± 0.05, respectively). Two effects may explain the difference observed between the patchy and continuous habitats: (i) patches in a patchy habitat have 4 sidewalls, whereas (virtual) patches in the continuous habitat only have 2, lowering the surface to volume ratio; (ii) patches in a patchy habitat have corners facilitating bacterial adhesion [40], while corners are absent in the continuous habitat. Both the increase in surface to volume ratio and the presence of corners, facilitate surface-associated growth. As a result, geometry-induced enhancement of surface-associated growth may be responsible for the increased persistence of prey we observe in the patchy habitat. While in our experiments the persisting bacteria did not divide, the exact physiological state of these remaining bacteria remains unknown. Assessing the capacity of these persisting prey to grow and divide will be of importance when utilizing *B. bacteriovorus* for water cleaning, crop protection, and as additional means to fight bacterial infections.

Acknowledgements

We thank Prof. Ran Nathan, Prof. Nadav Shnerb, Dr. R.W. Koster, Prof Liz Sockett, and several anonymous Reviewers (from several journals) for insightful comments.

Competing interests

We have no competing interests.

Authors' contributions

FJHH, DAK, EJ, and CD conceived and designed the experiments. FJHH and DAK performed experiments and analyzed the data. OR designed and contributed protocols. FJHH and DAK wrote the manuscript. All authors read and approved the final manuscript.

Funding

Supported by grants from the Minerva Foundation for Movement Ecology and the Dean of the faculty of Science of the Hebrew University to DAK. European Research Council grant NanoforBio No. 247072 and the Netherlands Organisation for Scientific Research (NWO/OCW) as part of the Frontiers of Nanoscience program to CD.

References

1. Dethlefsen, L., Eckburg, P. B., Bik, E. M. & Relman, D. A. 2006 Assembly of the human intestinal microbiota. *Trends Ecol. Evol.* **21**, 517–523. (doi:10.1016/j.tree.2006.06.013)

2. Stocker, R. 2012 Marine Microbes See a Sea of Gradients. *Science* **338**, 628–633. (doi:10.1126/science.1208929)

3. Ngom, N. F., Garnier, P., Monga, O. & Peth, S. 2011 Extraction of three-dimensional soil pore space from microtomography images using a geometrical approach. *Geoderma* **163**, 127–134.

4. Wolf, A. B., Vos, M., de Boer, W. & Kowalchuk, G. A. 2013 Impact of matric potential and pore size distribution on growth dynamics of filamentous and non-filamentous soil bacteria. *PloS One* **8**. (doi:10.1371/journal.pone.0083661)

5. Tilman, D. & Kareiva, P. M. 1997 *Spatial ecology: the role of space in population dynamics and interspecific interactions*. Princeton University Press.

6. Durrett, R. & Levin, S. 1994 The importance of being discrete (and spatial). *Theor. Popul. Biol.* **46**, 363–394.

7. Hanski, I. & Gaggiotto, O. 2004 *Ecology, Genetics, and Evolution of Metapopulations*. London, UK: Elsevier Academic Press.

8. Holyoak, M. & Lawler, S. P. 1996 Persistence of an extinction-prone predator-prey interaction through metapopulation dynamics. *Ecology* **77**, 1867–1879. (doi:10.2307/2265790)

9. Dey, S. & Joshi, A. 2006 Stability via asynchrony in Drosophila metapopulations with low migration rates. *Science* **312**, 434–436. (doi:10.1126/science.1125317)

10. Sutcliffe, O. L., Thomas, C. D., Yates, T. J. & GreatorexDavies, J. N. 1997 Correlated extinctions, colonizations and population fluctuations in a highly connected ringlet butterfly metapopulation. *Oecologia* **109**, 235–241. (doi:10.1007/s004420050078)

11. Ellner, S. P. et al. 2001 Habitat structure and population persistence in an experimental community. *Nature* **412**, 538–543. (doi:10.1038/35087580)

12. Earn, D. J. D., Levin, S. A. & Rohani, P. 2000 Coherence and Conservation. *Science* **290**, 1360–1364. (doi:10.1126/science.290.5495.1360)

13. Ben Zion, Y., Yaari, G. & Shnerb, N. M. 2010 Optimizing Metapopulation Sustainability through a Checkerboard Strategy. *PLoS Comput Biol* **6**, e1000643. (doi:10.1371/journal.pcbi.1000643)

14. Berg, H. C. 2000 Motile behavior of bacteria. *Phys. Today* **53**, 24–29. (doi:10.1063/1.882934)

15. Männik, J., Driessen, R., Galajda, P., Keymer, J. E. & Dekker, C. 2009 Bacterial growth and motility in sub-micron constrictions. *Proc. Natl. Acad. Sci.* **106**, 14861–14866.

16. Hall-Stoodley, L., Costerton, J. W. & Stoodley, P. 2004 Bacterial biofilms: from the Natural environment to infectious diseases. *Nat Rev Micro* **2**, 95–108. (doi:10.1038/nrmicro821)

17. Drescher, K., Shen, Y., Bassler, B. L. & Stone, H. A. 2013 Biofilm streamers cause catastrophic disruption of flow with consequences for environmental and medical systems. *Proc. Natl. Acad. Sci.* **110**, 4345–4350. (doi:10.1073/pnas.1300321110)

18. Keymer, J. E., Galajda, P., Muldoon, C., Park, S. & Austin, R. H. 2006 Bacterial metapopulations in nanofabricated landscapes. *Proc. Natl. Acad. Sci.* **103**, 17290–17295.

19. Connell, J. L., Ritschdorff, E. T., Whiteley, M. & Shear, J. B. 2013 3D printing of microscopic bacterial communities. *Proc. Natl. Acad. Sci.* **110**, 18380–18385. (doi:10.1073/pnas.1309729110)

20. Hol, F. J. H. & Dekker, C. 2014 Zooming in to see the bigger picture: microfluidic and nanofabrication tools to study bacteria. *Science* **346**. (doi:10.1126/science.1251821)

21. Hol, F. J. H., Hubert, B., Dekker, C. & Keymer, J. E. 2015 Density-dependent adaptive resistance allows swimming bacteria to colonize an antibiotic gradient. *ISME J.* (doi:10.1038/ismej.2015.107)

22. Lambert, C., Evans, K. J., Till, R., Hobley, L., Capeness, M., Rendulic, S., Schuster, S. C., Aizawa, S.-I. & Sockett, R. E. 2006 Characterizing the flagellar filament and the role of motility in bacterial prey-penetration by Bdellovibrio bacteriovorus. *Mol. Microbiol.* **60**, 274–286. (doi:10.1111/j.1365-2958.2006.05081.x)

23. Sockett, R. E. 2009 Predatory lifestyle of Bdellovibrio bacteriovorus. *Annu. Rev. Microbiol.* **63**, 523–539.

24. Fenton, A. K., Lambert, C., Wagstaff, P. C. & Sockett, R. E. 2010 Manipulating each MreB of Bdellovibrio bacteriovorus gives diverse morphological and predatory phenotypes. *J. Bacteriol.* **192**, 1299–1311.

25. Shemesh, Y. & Jurkevitch, E. 2004 Plastic phenotypic resistance to predation by Bdellovibrio and like organisms in bacterial prey. *Environ. Microbiol.* **6**, 12–18.

26. Kim, E.-H., Dwidar, M., Mitchell, R. J. & Kwon, Y.-N. 2013 Assessing the effects of bacterial predation on membrane biofouling. *Water Res.* **47**, 6024–6032. (doi:10.1016/j.watres.2013.07.023)

27. Sockett, R. E. & Lambert, C. 2004 Bdellovibrio as therapeutic agents: a predatory renaissance? *Nat Rev Micro* **2**, 669–675. (doi:10.1038/nrmicro959)

28. Fratamico, P. & Whiting, R. 1995 Ability of Bdellovibrio Bacteriovorus 109J to lyse Gram-negative food-borne pathogenic and spoilage bacteria. *J. Food Prot.* **58**, 160–164.

29. Fratamico, P. M. & Cooke, P. H. 1996 Isolation of Bdellovibrios that prey on Eschericha Coli O157:H7 and Salmonella species and application for removal of prey from stainless steel surfaces. *J. Food Saf.* **16**, 161–173. (doi:10.1111/j.1745-4565.1996.tb00157.x)

30. Lambert, C., Smith, M. C. M. & Sockett, R. E. 2003 A novel assay to monitor predator-prey interactions for Bdellovibrio bacteriovorus 109 J reveals a role for methyl-accepting chemotaxis proteins in predation. *Environ. Microbiol.* **5**, 127–132.

31. Jurkevitch, E., Minz, D., Ramati, B. & Barel, G. 2000 Prey range characterization, ribotyping, and diversity of soil and rhizosphere Bdellovibrio spp. isolated on phytopathogenic bacteria. *Appl. Environ. Microbiol.* **66**, 2365–2371.

32. STOLP, H. & STARR, M. P. 1963 BDELLOVIBRIO BACTERIOVORUS GEN. ET SP. N., A PREDATORY, ECTOPARASITIC, AND BACTERIOLYTIC MICROORGANISM. *Antonie Van Leeuwenhoek* **29**, 217–248.

33. Shanks, R. M. Q., Davra, V. R., Romanowski, E. G., Brothers, K. M., Stella, N. A., Godboley, D. & Kadouri, D. E. 2013 An Eye to a Kill: Using Predatory Bacteria to Control Gram-Negative Pathogens Associated with Ocular Infections. *PLoS ONE* **8**, e66723. (doi:10.1371/journal.pone.0066723)

34. Monnappa, A. K., Dwidar, M., Seo, J. K., Hur, J.-H. & Mitchell, R. J. 2014 Bdellovibrio bacteriovorus Inhibits Staphylococcus aureus Biofilm Formation and Invasion into Human Epithelial Cells. *Sci. Rep.* **4**. (doi:10.1038/srep03811)

35. Hol, F. J. H., Galajda, P., Nagy, K., Woolthuis, R. G., Dekker, C. & Keymer, J. E. 2013 Spatial Structure Facilitates Cooperation in a Social Dilemma: Empirical Evidence from a Bacterial Community. *PLoS ONE* **8**, e77042. (doi:10.1371/journal.pone.0077042)

36. Edelstein, A., Amodaj, N., Hoover, K., Vale, R. & Stuurman, N. 2010 Computer Control of Microscopes Using μManager. *Curr Protoc Mol Biol* (doi:10.1002/0471142727.mb1420s92)

37. Park, S., Kim, D., Mitchell, R. J. & Kim, T. 2011 A microfluidic concentrator array for quantitative predation assays of predatory microbes. *Lab. Chip* **11**, 2916–2923. (doi:10.1039/C1LC20230H)

38. van Vliet, S., Hol, F. J. H., Weenink, T., Galajda, P. & Keymer, J. E. 2014 The effects of chemical interactions and culture history on the colonization of structured habitats by competing bacterial populations. *BMC Microbiol.* **14**. (doi:10.1186/1471-2180-14-116)

39. Kadouri, D. E. & O'Toole, G. A. 2005 Susceptibility of Biofilms to Bdellovibrio bacteriovorus Attack. *Appl Env. Microbiol* **71**, 4044–4051. (doi:10.1128/AEM.71.7.4044-4051.2005)

40. Friedlander, R. S., Vlamakis, H., Kim, P., Khan, M., Kolter, R. & Aizenberg, J. 2013 Bacterial flagella explore microscale hummocks and hollows to increase adhesion. *Proc. Natl. Acad. Sci.* **110**, 5624–5629. (doi:10.1073/pnas.1219662110)

Figure captions

Figure 1.

On-chip predator-prey system. (a). Soil consists of a three-dimensional network of micron-sized patches. (b). A control experiment, in which only prey is introduced to a patchy landscape, consisting of coupled patches (top). A heatmap of a kymograph (depicting space horizontally and time vertically) showing the population dynamics of fluorescently labeled *E. coli* in log-scale. (c) The mean prey growth dynamics over all patches shows the familiar phases of bacterial growth: exponential phase and entry into stationary phase (at t=10h). (d, e) Predator-prey dynamics in the presence of predator in a patchy landscape (d) and a "continuous" landscape (e). Software-generated "virtual" patches that are used in data analysis of the continuous habitat are indicated by red dashed lines. In both habitats there initially is a steep rise in fluorescence which corresponds to growth of *E. coli*, followed by a death phase in which *E. coli* lyse after predation. Each pixel represents a single habitat patch. Microscopy images show representative snapshots of the population dynamics in phases i - iv, arrows indicate the approximate space and time of image acquisition.

Figure 2.

Predation rates in a patchy landscape. (a) Yellow dots indicate 98x98 points (for clarity, only 16x16 are shown) that were used to generate time traces (thin blue lines show single time traces for one patch, the fat black line represents the mean) from patches of the fragmented landscape. The maximum predation rate is extracted from individual traces. (b) Distribution of the maximal rate of decay of four patches. (c) All time traces of all patches within a patchy habitat (thin red lines show single time traces for one patch, the fat black line represents the mean). (d) The distributions of the maximum decay rates calculated for all points in all patches within the patchy landscape.

Figure 3.

Predation rates in the continuous landscape. (a) Yellow dots indicate 98x98 points (for clarity, only 16x16 are shown) that were used to generate time traces (thin blue lines show single time traces for one virutal patch, the fat black line represents the mean) from patches of the continuous landscape. The maximum predation rate is extracted from individual traces. (b) Distribution of the maximal rate of decay of four virtual patches. (c) All time traces of all virtual patches within a continuous habitat (thin red lines show single time traces for one patch, the fat black line represents the mean). (d) The distributions of the maximum decay rates calculated for all points in all virtual "patches" within the continuous landscape.

603 Figure 4

604 Correlation in patchy and continuous habitats. (a) The temporal correlation of the population
605 dynamics decreases with increasing patch distance. Beyond approximately 15 patches,
606 correlation in the patchy landscape (red) is lost more rapidly than in the continuous landscape
607 (black). (b) Kaplan-Meier survival functions for a patchy landscape (red) and a continuous
608 landscape (black). The two functions differ (p<0.00001) and the fraction of prey population
609 that remains in the patchy landscape is higher than in the continuous landscape (p=0.05), see
610 Results).